Asian Journal of Chemistry; Vol. 27, No. 8 (2015), 2917-2923

ASIAN JOURNAL OF CHEMISTRY

http://dx.doi.org/10.14233/ajchem.2015.18288

Electrochemical and Quantum Chemical Assessment of 2-Aminothiazole as Inhibitor for Carton Steel in Sulfuric Acid Solution

LEI GUO[1], SHANHONG ZHU[2], WENPO LI[1,*] and SHENGTAO ZHANG[1]

[1]School of Chemistry and Chemical Engineering, Chongqing University, Chongqing 400044, P.R. China
[2]School of Computer and Information Engineering, Xinxiang University, Xinxiang 453003, P.R. China

*Corresponding author: Tel/Fax: +86 23 65112804; E-mail: cqliwp@163.com

Received: 10 June 2014; *Accepted*: 1 September 2014; *Published online*: 27 April 2015; AJC-17163

Inhibition action of 2-aminothiazole towards carton steel corrosion in 0.1 M H_2SO_4 solution was investigated by electrochemical measurements. Quantum chemical calculations based on the density functional theory were performed on 2-aminothiazole. The polarization measurements show that 2-aminothiazole is arranged as a mixed-type inhibitor for both anodic and cathodic reactions. The surface morphology of uninhibited and inhibited carton steel sample was examined by scanning electron microscope. Moreover, a low-coverage gas-phase adsorption of 2-aminothiazole on perfect Fe(110) surface has been studied and characterized using density functional theory calculations.

Keywords: Electrochemical investigation, Corrosion inhibitor, 2-Aminothiazole, Carton steel, Density function theory.

INTRODUCTION

Corrosion is the destructive attack of metal or alloy chemically or electrochemically against its environment which leads to the loss of useful properties of materials. Several approaches have been proposed to minimize or prevent metal dissolution; one of these approaches is the use of substances called corrosion inhibitors[1-3]. Inhibitors can adhere to a metal surface to form a protective barrier against corrosive agents in contact with metal. The effectiveness of an inhibitor to provide corrosion protection depends to a large extent on the interaction between the inhibitor and the metal surface. Most well-known acid inhibitors are organic compounds with π-electrons and functional groups containing heteroatoms which can donate lone-pair electrons[4].

Clarification of the interaction between inhibitor molecules and surface metal atoms at the molecular level is important in terms of finding new and effective inhibitors. Quantum chemical calculations are proved to be a very powerful tool for studying the inhibition mechanism[5-7]. Adsorption-related electronic properties, adsorption geometries and energies, charge transferred from or toward the surface or a full description of the bonding electronic structure, are useful and can be achieved by means of density function theory methodology. 2-Aminothiazole is a heterocyclic organic compound with different anchoring sites suitable for surface bonding: nitrogen atom with its lone sp^2 electron pair, the sulfur atom, the amino group with its lone pair of electron, the -C=C-"edge" and the aromatic ring. So it is therefore a potentially effective inhibitor. To facilitate the presentation the Lewis structure of 2-aminothiazole along with the numbering of atoms is presented in Fig. 1.

The objective of the present work was to first investigate the effect of 2-aminothiazole on the corrosion of carton steel corrosion in 0.1 M H_2SO_4 solution using electrochemical method and to subsequently clarify its interaction with the Fe(110) surface at the molecular level by density functional theory calculations.

EXPERIMENTAL

Materials and sample preparation: The corrosion tests were performed on carton steel of the following composition: 0.45 % C, 0.20 % Si, 0.70 % Mn, 0.25 % Cr and the remained is Fe. 2-Amino thiazole was dissolved in 0.1 M H_2SO_4 at different concentrations (from 300 to 700 mg/L). The solution in the absence of 2-aminothiazole was taken as blank for comparison.

The sizes for surface analysis were 1 cm × 1 cm × 0.5 cm, while, for electrochemical experiments, the specimens were embedded in epoxy resin with a geometrical surface area of 1 cm^2 exposed to the electrolyte. Before each electrochemical measurement, the specimen was mechanically ground up to 1000 grit emery paper, then washed in deionized water and immediately dried with air.

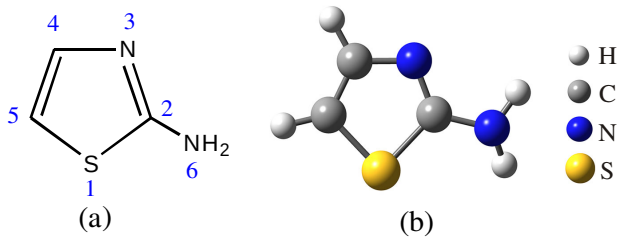

Fig. 1. (a) Lewis structure and (b) ball and stick model of 2-aminothiazole. Numbering and coloring of atoms is also indicated

Electrochemical test: The electrochemical studies were carried out with CHI604D electrochemical workstation (Shanghai Chenhua CO., LTD) in a traditional three-electrode cell at 298 K. A platinum sheet and a saturated calomel electrode (SCE) were used as auxiliary and reference electrode, respectively. All potentials were referred to saturated calomel electrode reference electrode. Electrochemical impedance spectroscopy (EIS) measurements were carried out at the open circuit potential (E_{OCP}). The alternating current frequency range extended from 10^{-2} to 10^{5} Hz with 5 mV amplitude. Then the impedance data were analyzed and fitted. The potentiodynamic polarization curves were obtained from -250 mV to + 250 mV *versus* E_{OCP} with a sweep rate of 2 mV s^{-1}. Each experiment was repeated at least three times to check the reproducibility.

SEM analysis: The surface morphology of specimens after immersion in 0.1 M H_2SO_4 in the absence and presence of 2-aminothiazole was performed on a KYKY2800B scanning electron microscope. The accelerating voltage was 25 kV.

Computational details: The density functional theory calculations for the 2-aminothiazole molecule were accomplished by means of the Gaussian 03 program to analyze the structural and electronic parameters. The structures were fully optimized and vibrational analyses were carried out to verify that the optimized geometries corresponded to minimum global energy. The popular Becke's three-parameter hybrid functional (B3LYP)[8] method in combination with the 6-311++G(d,p) basis set has been chosen. To better clarify the nature of the intermolecular (X = S and N) contact in the formed Fe-inhibitor complex, several possible Fe-2-aminothiazole structures were optimized at B3LYP/GENECP level (LANL2DZ[9] basis set for Fe). The atoms in molecules (AIM)[10] theory has been employed on basis of the optimized structures.

Furthermore, the supercell approach was also employed to describe the covalent interaction between 2-aminothiazole and the Fe(110) surface in a simulation box (9.9 × 9.9 × 33.1 Å) with periodic boundary conditions. The Fe(110) was first built and relaxed. The surface area was increased and its periodicity was changed by constructing a 5-layer 4 × 4 supercell, with a vacuum slab of thickness 25 Å. The three bottom layers of the slab were kept frozen to the bulk positions, while all other degrees of freedom were relaxed. Spin-polarized density functional theory calculations were performed in the framework of generalized gradient approximation (GGA) of Perdew-Burke-Ernzerhof (PBE)[11] using the linear combination of atomic orbitals (LCAO) method with effective core pseudopotentials (ECPs)[12] as implemented in the $Dmol^3$ code of the Materials Studio software (Accelrys Inc.)[13]. The valence electron functions were expanded into a set of numerical atomic orbits by a double-numerical basis with polarization functions (DNP)[14]. Brillouin-zone integrations were performed using 3 × 3 × 1 *k*-point grid which was generated automatically using the Monkhorst-Pack method. The tolerances of energy, gradient and displacement convergence were 1×10^{-5} Ha, 2×10^{-3} Ha/Å and 5×10^{-3} Å, respectively.

The lattice constant of bulk bcc Fe was calculated to be 2.89 Å, in good agreement with previous theoretical[15] and experimental work[16]. At this lattice constant, the total magnetization was found to be 2.60 μB per atom once again in good agreement with previous work[17,18]. The total magnetic moment per atom of the five-layer slab was calculated to be 2.72 μB in ferromagnetic order. Adsorption energies are calculated using the formula:

$$E_{ads} = E_{Mol/surf} - (E_{surf} + E_{Mol}) \quad (1)$$

where E_{Mol}, E_{surf} and $E_{Mol/surf}$ are the total energies of isolated adsorbate, Fe(110) slab and Mol/Fe(110) system, respectively. Based on this definition, a negative value of E_{ads} corresponds to a stable adsorption structure. In order to investigate the changes of electronic structures when the adsorbates chemisorbed on the Fe(110) surface, deformation charge density Δρ(r) was calculated. The transfer of electron density between two atoms was analyzed. Δρ(r) is defined as

$$\Delta\rho(r) = \rho_{total}(r) - \sum \rho_{atom}(t) \quad (2)$$

where $\rho_{total}(r)$ and $\rho_{atom}(r)$ are electron density of the adsorbate-surface adsorption system and individual isolated atom, respectively.

RESULTS AND DISCUSSION

Potentiodynamic polarization measurements: The representative potentiodynamic polarization curves of the carton steel electrode, which were obtained in 0.1 M H_2SO_4 solution in the absence and presence of various concentrations of 2-aminothiazole are given in Fig. 2. In order to obtain information about the kinetics of the corrosion, two electrochemical parameters, *i.e.*, corrosion potential (E_{corr}) and corrosion current density (i_{corr}) values were calculated from the corresponding polarization curves and the obtained data are given in Table-1. The inhibition efficiency (η_p) was calculated using the following equation:

$$\eta_p = \frac{i_{corr(0)} - i_{corr(inh)}}{i_{corr(0)}} \times 100 \quad (3)$$

where $i_{corr(0)}$ and $i_{corr(inh)}$ represent corrosion current density values without and with inhibitor, respectively. The i_{corr} values were determined by the extrapolation of the linear portions of the Tafel curves to the corresponding corrosion potentials.

Fig. 2 and Table-1 show that the addition of the inhibitor to the H_2SO_4 solution reduces both anodic metal dissolution and cathodic hydrogen evolution reactions, as expected. The reduction in i_{corr} is pronounced more and more with the increasing inhibitor concentration. It has been observed that 600 mg/L of 2-aminothiazole serves as an optimum concentration that exhibit higher efficiency of corrosion inhibition. The results indicated that inhibitor is concentration-independent

TABLE-1
POTENTIODYNAMIC POLARIZATION AND ELECTROCHEMICAL IMPEDANCE PARAMETERS FOR CATON STEEL IN 0.1 M H_2SO_4 WITH DIFFERENT CONCENTRATIONS OF 2-AMINOTHIAZOLE 298 K

C_{inh} (mg/L)	Tafel			EIS				
	E_{corr} (mV)	i_{corr} (μA cm^{-2})	η_p	R_s (Ω cm^2)	R_{ct} (Ω cm^2)	C_{dl} (μF cm^{-2})	n	η_R
Blank	-520	298.1	/	2.36	55.1	151.9	0.932	/
300	-496	120.6	59.56	2.81	115.5	96.57	0.931	52.3
400	-500	86.9	70.83	2.20	159.8	83.74	0.922	65.5
500	-491	74.6	74.98	3.65	190.3	76.15	0.930	70.9
600	-492	63.4	78.79	2.56	224.1	59.95	0.934	75.4
700	-501	71.4	75.14	2.89	202.5	64.85	0.915	72.8

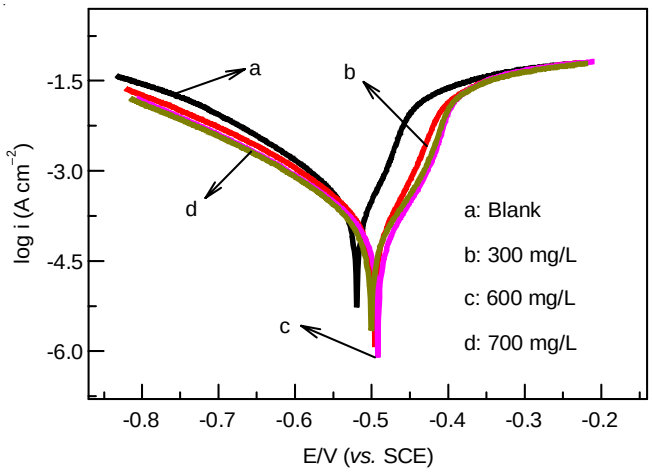

Fig. 2. Polarization curves for carton steel in 0.1 M H_2SO_4 with different concentrations of 2-aminothiazole

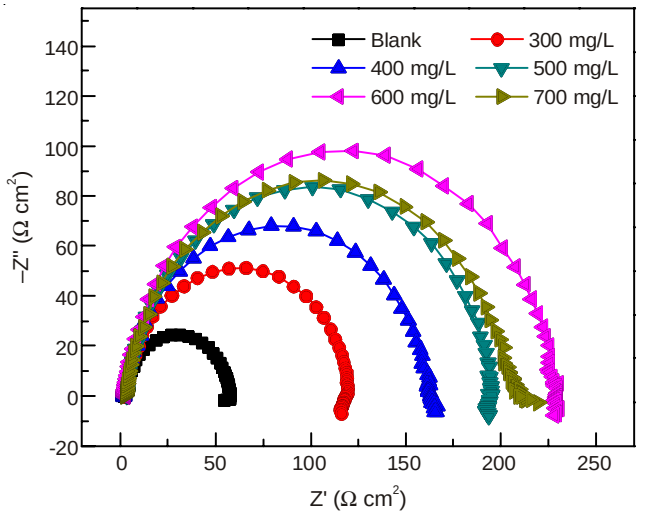

Fig. 3. Nyquist diagrams for carbon steel in 0.1 M H_2SO_4 containing different concentrations of 2-aminothiazole

as inhibition efficiency decrease at highest concentration. The increased inhibition efficiency with the inhibitor concentration indicates that the tested organic compound acts by adsorbing on the carton steel surface. The presence of 2-aminothiazole in 0.1 M H_2SO_4 solution shifts the corrosion potential slightly towards more positive potentials with respect to the corrosion potential observed in the absence of the inhibitor. The maximum displacement in E_{corr} value was 29 mV (< 85 mV) for 2-aminothiazole which indicates that the inhibitors acts as mixed-type inhibitor with predominant anodic effectiveness[19]. The cathodic polarization curves in Fig. 2 are giving rise to parallel lines. This shows that the addition of 2-aminothiazole to the 0.1 M H_2SO_4 solution does not affect the mechanism of hydrogen-reduction of H^+ ions to H_2 through charge transfer[20]. The inhibition effect of 2-aminothiazole may be caused by the simple blocking effect, namely the reduction of reaction area on the corroding surface. It is important to note that the presence of inhibitor does not change the current-potential characteristics in anodic domain for potential higher than approximate -0.4 V. This potential can be defined as the desorption potential. Similar results have been reported with N-heterocyclic compound inhibitors in acidic solution[21-23]. In that case, the inhibition of corrosion depends on the potential of electrode. Thus, the behavior of 2-aminothiazole at potentials greater than -0.4 V could be associated to the significant dissolution of steel.

Electrochemical impedance spectroscopy (EIS): Nyquist impedance diagrams are shown in Fig. 3 at various inhibitor concentrations. It can be observed that all impedance spectra show a single depressed capacitive loop which is related to charge transfer of the corrosion process. The capacitive loops are not perfect semicircles which can be attributed to the frequency dispersion effect as a result of the roughness and inhomogeneous of electrode surface[24,25]. The equivalent circuit model used to fit the experimental results is shown in Fig. 4. R_s is the resistance of the solution between the working electrode and the reference electrode and R_{ct} represents the charge-transfer resistance whose value is a measure of electron transfer across the surface[26]. The constant phase element (CPE) has the value of the frequency-distributed double-layer capacitance. The impedance function of the CPE is represented by the expression

$$Z_{CPE} = Y_0^{-1}(j\omega)^{-n} \quad (4)$$

where Y_0 is a proportionality coefficient, ω is the angular frequency (in rad s^{-1}) and $j^2 = -1$ is the imaginary number, *n* is the exponent related to the phase shift and can be used as a measure of the surface inhomogeneity[27]. While n = 0, the CPE represents a pure resistor, for n = -1 an inductor and for n = + 1, a pure capacitor[28]. The values of the double layer capacitance (C_{dl}) and inhibition efficiency (η_R) are calculated as follow:

$$C_{dl} = \left(Y_0 \times R_{ct}^{1-n}\right)^{1/n} \quad (5)$$

$$\eta_R = \frac{R_{ct(inh)} - R_{ct(0)}}{R_{ct(inh)}} \times 100 \quad (6)$$

where $R_{ct(0)}$ and $R_{ct(inh)}$ are the charge transfer resistance in the absence and presence of the inhibitor, respectively.

The satisfactory fit was obtained for all experimental data with this model. The fitted parameter results are presented in Table-1. It can be seen from this table that the solution resistance is very small and thus can be negligible. The increase in concentration of the inhibitor results in higher R_{ct} which indicates the enhancement of the adsorbed 2-aminothiazole film on the carton steel surface and blocking the surface against to charge and mass transfer more efficiently. When the concentration of 2-aminothiazole was 600 mg/L, the capacitive reactance arc radius reached the largest. After that, when we continued increasing the concentration of the 2-aminothiazole, the capacitive reactance arc radius decreased sharply, then the corrosion inhibition efficiency decreased. This is basically consistent with previous tafel analysis. According to the well known Helmholtz model[29,30]:

$$C_{dl} = \frac{\varepsilon^0 \varepsilon}{d} S \quad (7)$$

where d is the thickness of the protective layer, ε^0 is the permittivity of the air, ε is the local dielectric constant and S is the electrode surface area. The increase in thickness of the double layer was confirmed by the decrease in double layer capacitance values, which in turn justify that the inhibitor reduces the metal dissolution by effective adsorption.

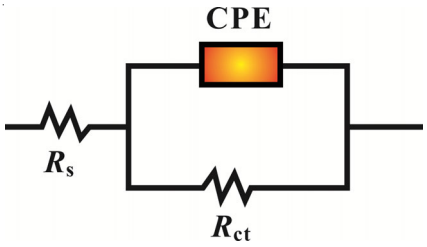

Fig. 4. Equivalent circuit model used to fit the EIS experiment data

SEM analysis: The surface morphology of carbon steel samples immersed in 0.1 M H_2SO_4 solutions for 6 h at 298 K without and containing optimum concentration of 2-aminothiazole was studied by SEM. As shown in Fig. 5, the steel sample before immersion seems smooth (Fig. 5a). In the presence of 2-aminothiazole, the surface of the specimen (Fig. 5b) is well protected. In contrast, the specimen surface in the absence of 2-aminothiazole is severely corroded and the surface becomes porous and rough (Fig. 5c). These results indicate that the corrosion of carton steel in 0.1 M H_2SO_4 solution is inhibited remarkably by 2-aminothiazole.

Theory study: Bond lengths and Mayer-Mulliken bond orders (BOs) for the optimized 2-aminothiazole are summarized in Table-2. It can be observed that the bond orders are in the 1.82-0.62 range. In consistency with the calculated

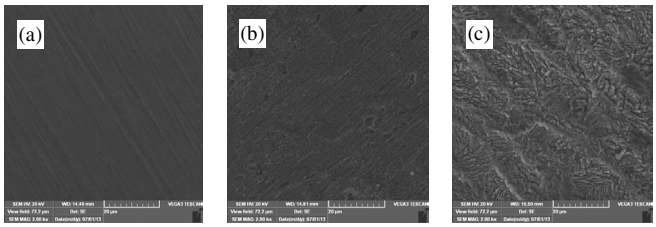

Fig. 5. SEM micrographs of (a) freshly polished carton steel specimen and the specimens immersed in 0.1 M H_2SO_4 solution for 6 h with 600 mg/L 2-aminothiazole (b) and without 2-aminothiazole (c)

equilibrium bond lengths, these bond order values suggest a moderate aromatic character for the five-member ring of thiazole. The C2-N3 (C4-C5) bond distance of around 1.29 Å (1.35 Å) implies a double bond, also confirmed by the calculated bond order.

Frontier orbital theory was useful in predicting the adsorption centers of the inhibitor molecule responsible for the interaction with surface metal atoms[31]. It is generally acknowledged that in addition to HOMO and LUMO orbitals at least few other high lying occupied molecular orbitals (MO) – those lying at the position of the metal *d*-band – should be considered to describe the molecule-surface bonding upon adsorption, because these molecular orbitals will likely hybridize with metal *d*-states[32]. In Fig. 6, four frontier occupied molecular orbitals HOMO-2, HOMO-1, HOMO and LUMO (where HOMO-*n* means *n*th MO below the HOMO) are provided. The corresponding orbital contributions (except Rydberg compositon) of the non-hydrogen atoms were calculated using the Multiwfn software[33] and the results are tabulated in Table-3. We can see that HOMO is π-type and is spread through the whole molecule. The N3 and S1 atoms, which have lone pairs of electrons for donation, contribute greatly to the HOMO-1 and HOMO-2, respectively.

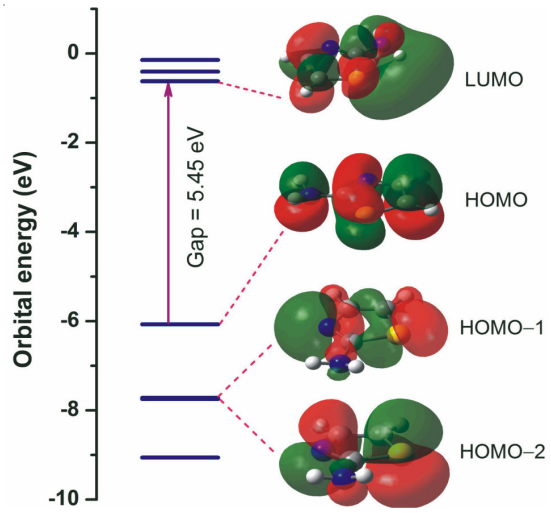

Fig. 6. Frontier molecular orbitals of 2-aminothiazole in particular HOMO·2, HOMO·1, HOMO and LUMO are plotted

TABLE-2
CALCULATED BOND LENGTHS (IN Å) AND MAYER BOND ORDERS OF 2-AMINOTHIAZOLE

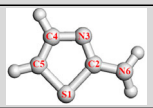

	S1-C2	C2-N3	N3-C4	C4-C5	C5-S1	C2-N6
Bond length	1.7678	1.2986	1.3788	1.3565	1.7497	1.3768
Bond order	0.8193	1.6790	1.0014	1.8228	0.6223	1.1733

TABLE-3
ORBITAL COMPOSITION ANALYSIS BY NATURAL ATOMIC ORBITAL (NAO) METHOD

Atom	HOMO		HMOM-1		HOMO-2		LUMO	
	Type	Composition (%)	Type	Composition (%)	Type	Composition (%)	Type	Composition (%)
S1	$3p_z$	10.40	3p	17.16	$3p_z$	51.62	3p	11.26
C2	$2p_z$	11.48	2py	0.95	2p	0.12	$2p_z$	15.81
N3	$2p_z$	9.63	2s, 2p	72.85	$2p_z$	28.48	$2p_z$	2.98
C4	$2p_z$	16.01	2s, 2p	1.93	$2p_z$	7.66	$2p_z$	7.57
C5	$2p_z$	27.32	2s, 2p	2.97	$2p_z$	4.06	$2p_z$	14.07
N6	$2p_z$	21.97	2s, 2p	1.48	$2p_z$	1.52	2s, 2p	5.02

As displayed in Fig. 7, the interaction modes adopted for 2-aminothiazole can be classified into two types overall. For the Fe-N6 and Fe-S1 modes, the Fe atom is almost perpendicular to the thiazole ring of 2-aminothiazole, where the calculated tilting angles are 119.2° and 127.4°, respectively. Therefore, most probably, 2-aminothiazole should be adsorbed parallel to the Fe surface in the realistic condition, facilitating the additional orbital interaction between the *d*-orbital of Fe and the π antibonding orbital of 2-aminothiazole. On the other hand, for Fe-N3 mode, the Fe atom and the aromatic ring are almost coplanar, suggesting that it is probably adsorbed perpendicular to the Fe surface through the only σ-orbital interaction between the lone pair electrons of N3 atom of 2-aminothiazole and Fe atom.

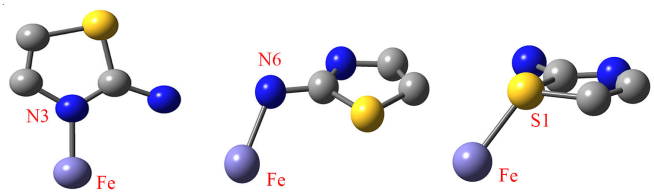

Fig. 7. Optimized Fe-AT complexes formed by different contact methods

Bader's quantum theory of AIM is based on topological analysis of the total electron density and hence gives a description of the bonding which is in many respects complementary to the MO analysis. In the AIM analyses, the existence of the interatomic interaction is indicated by the presence of a so-called bond critical point (BCP). It is a common practice to use the values of certain descriptors at bond critical points to characterize the bonding between the atoms, such as the electron density (ρ_{bcp}), its Laplacian (L_{bcp}), the total energy density (H_{bcp}) and absolute ratio of potential and kinetic energies densities ($|V_{bcp}|/G_{bcp}$). Macchi and Sironi[34] have summarized that the covalent bonds involving transition metals are characterized by: (i) the small values of H_{bcp} and L_{bcp}; (ii) negative total energy density $H_{bcp} < 0$ (that is, in covalent bonds the potential energy is dominated over kinetic energy). Espinosa *et al.*[35] proposed use of the $|V_{bcp}|/G_{bcp}$ ratio to classify different types of interactions: this ratio is less than 1 ($L_{bcp} > 0$ and $H_{bcp} > 0$) for the pure closed-shell interactions, $|V_{bcp}|/G_{bcp}$ is more than 2 ($L_{bcp} < 0$ and $H_{bcp} < 0$) for the pure open-shell (covalent) interactions, while the bonds with $1 < |V_{bcp}|/G_{bcp} < 2$ ($L_{bcp} > 0$ and $H_{bcp} < 0$) were defined as "intermediate". The corresponding topological parameters at the bond critical points for the three modes in Fig. 7 have been presented in Table-4. As expected, these parameters revealed a covalent character between Fe and 2-aminothiazole. The calculated Fe-X bond distance is about 2 Å, being close to the sum of N/S and Fe covalent radii. A net electron transfer from 2-aminothiazole to Fe has been observed for Fe-N3, Fe-N6 and Fe-S1, where the corresponding magnitudes are 0.139, 0.137 and 0.133, respectively.

To further seek the most stable adsorption configuration, the adsorption behavior of 2-aminothiazole on the Fe(110) surface have been investigated employing periodic slab models. Three stable adsorption configurations were identified and are shown in Fig. 8, together with their respective adsorption energies. The adsorption energy of the parallel adsorption configuration (left panel of Fig. 8) is -1.739 eV, which is more exothermic than presently reported adsorption energy for single water molecule on Fe(110) (*e.g.*, -0.26 eV)[36]. Actually, the adsorption of organic inhibitor molecules from the aqueous solution can be considered as a quasi-substitution process between the organic compounds in the aqueous phase [$Org_{(sol)}$] and water molecules associated with the metallic surface [$H_2O_{(ads)}$] as represented by the following equilibrium[37]:

$$Org_{(sol)} + xH_2O_{(ads)} \rightarrow Org_{(ads)} + xH_2O_{(sol)} \quad (8)$$

where x is the number of water molecules replaced by one organic molecule. Thus, the calculation results indicate that the water molecules can be easily substituted by 2-aminothiazole adsorbate. For the configuration in the central panel of Fig. 8, the S1 atom is bonded simultaneously to two adjacent Fe atoms. This form is analogous to the methionine adsorption on Fe(110) surface[38]. A third adsorption configuration was identified in which the molecular plane of 2-aminothiazole is perpendicular to the surface (right panel of Fig. 8). In this case, the interaction between the surface and 2-aminothiazole is only through the N3 atom of the the surface Fe atom directly

TABLE-4
CALCULATED TOPOLOGICAL PARAMETERS AT THE BCPs OF THE Fe....X (X = N OR S) CONTACTS AS WELL AS NPA ATOMIC CHARGES ON THE Fe ATOM (q_{Fe})

Mode	BCP	ρ_{bcp}	L_{bcp}	H_{bcp}	$\lvert V_{bcp}\rvert/G_{bcp}$	$R_{Fe...X}$ (Å)	q_{Fe}
I	Fe...N3	0.1007	0.5455	-0.0296	1.179	1.9132	-0.139
II	Fe...N6	0.0881	0.4918	-0.0212	1.147	1.9655	-0.137
III	Fe...SI	0.0947	0.3547	-0.0285	1.243	2.1226	-0.133

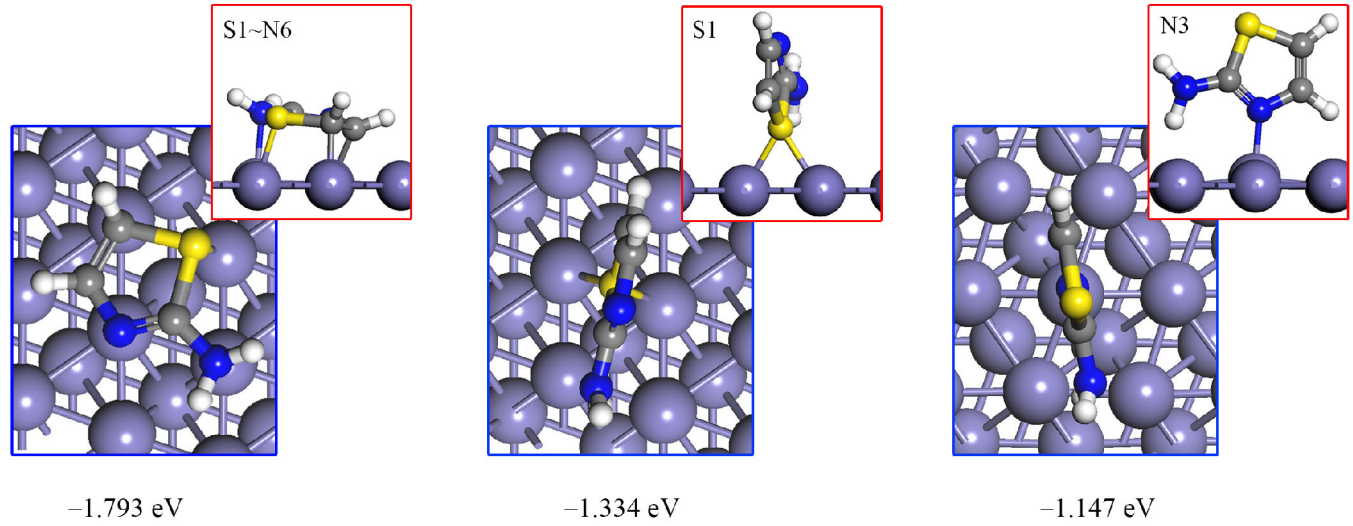

Fig. 8. Three stable adsorption configurations (top view) of 2-aminothiazole on Fe(110) surface together with their adsorption energies (insets: side view)

beneath it, which is displaced by approximately 0.22 Å in the direction of the surface normal. The computed adsorption energy (-1.147 eV) is a bit low compared to the parallel configuration, mainly because the π-molecular orbitals are involved in the interaction in the latter configuration.

The deformation electron density for all three adsorption configurations are shown in the upper panels of Fig. 9. Red and blue regions indicate the electron accumulation and depletion, respectively. It is observed that the electron density is depleted from 2-aminothiazole molecule and accumulates on the Fe atoms (red area), which indicates the formation of the covalent bonds. Hirshfeld charge analysis shows that the total charge of each adsorbed 2-aminothiazole molecule is positive and the values are 0.116 e, 0.054 e and 0.085 e for the three configurations from left to right. The large value of the adsorption energy for the flat configuration are apparently a consequence of the strong interaction of the delocalized π-electrons of the thiazole ring with the surface Fe atoms. This is further corroborated from the analysis of the density of states (DOS) given in the lower panels of Fig. 9. The molecular density of state is relatively unstructured in the vicinity of the Fermi energy for this parallel configuration. This behavior is different from the perpendicular adsorption configurations, in which the 2-aminothiazole density of states show sharp peaks at the overlapping areas. Similar results have been obtained for another corrosion inhibitior in acid media[39].

Mechanism of adsorption and inhibition: A general mechanism for the dissolution of carton steel in H_2SO_4 solution would be similar to that reported in the literature[40]:

$$Fe + SO_4^{2-} \leftrightarrow (FeSO_4)_{ads} + 2e^- \quad (9)$$

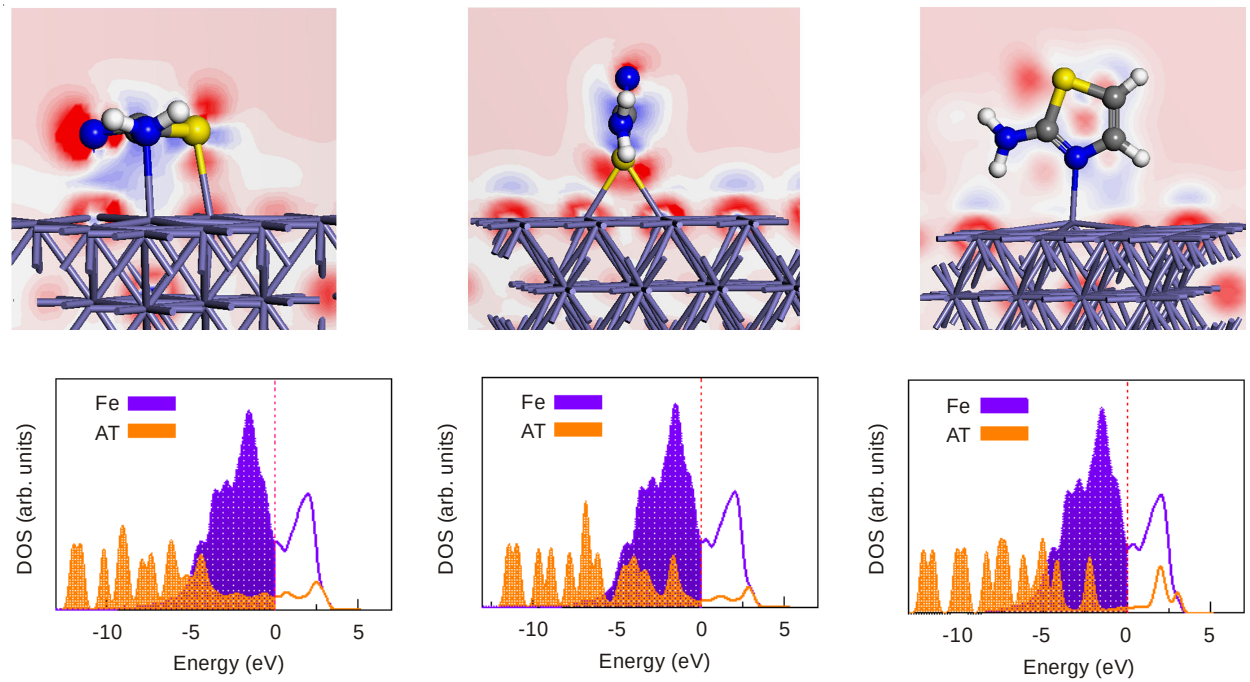

Fig. 9. Deformation electron density (upper panels) and density of states projected to 2-aminothiazole and Fe (lower panels) for the three stable adsorption configurations in Fig. 8

$$(FeSO_4)_{ads} \leftrightarrow Fe(II) + SO_4^{2-} \quad (10)$$

However, for specimens in the inhibited H_2SO_4 solutions, the [Fe(0)AT] complex is formed at the flat area *via* the following reaction:

$$AT + Fe(0) \rightarrow [Fe(0)AT] \quad (11)$$

Schematic representation of the proposed mode of adsorption of 2-aminothiazole molecule is shown in Fig. 10. It is shown that 2-aminothiazole (AT) can react with Fe(0) and forms a complete protective film in the cathodic area. This film is very thin and is probably a single monolayer. Generally, in the corroded area (*i.e.*, anodic area), the metal surface is positively charged. On the other hand, the 2-aminothiazole molecule may exist either as protonated form (ATH^+) or as neutral one in acid medium. Thus, the ATH^+ may adsorb on iron surface through synergistic effect with sulfate radical and forms a thick and protective [Fe ATH^+] complex, by which, the metal surface is protected against being attacked by corrosive ions.

The cathodic hydrogen evolution reaction may be given as follows[41]:

$$Fe + H^+ \leftrightarrow (FeH^+)_{ads} \quad (12)$$

$$(FeH^+)_{ads} + e^- \rightarrow (FeH)_{ads} \quad (13)$$

$$(FeH)_{ads} + H^+ + e^- \rightarrow Fe + H_2 \quad (14)$$

The protonated 2-aminothiazole molecules are also adsorbed at cathodic sites of carton steel in competition with hydrogen ions that going to reduce to H_2 gas evolution.

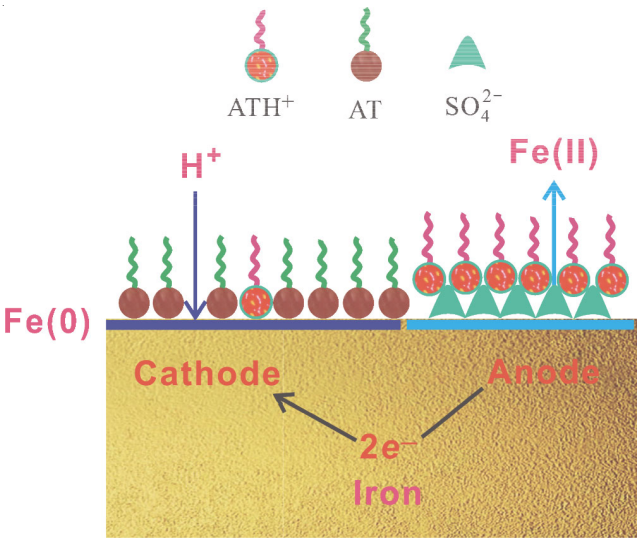

Fig. 10. Proposed scheme for the adsorption of 2-aminothiazole molecule on the iron surface in acid medium.

Conclusion

The corrosion of carton steel in a 0.1 M H_2SO_4 solution was inhibited by 2-aminothiazole to some extent in the concentration range studied. 2-Aminothiazole inhibits both the anodic and cathodic reactions by blocking the active corrosion sites on the steel surface and acts as a mixed type inhibitor. EIS results showed that as the inhibitor concentration increased the charge transfer resistance increased and the double layer capacity decreased. Three stable end configurations on the Fe(110) surface were theoretically identified for 2-aminothiazole, with the parallel adsorption configuration being the most stable.

ACKNOWLEDGEMENTS

This research was sponsored by the National Natural Science Foundation of China (21376282).

REFERENCES

1. M.M. Antonijevic and M.B. Petrovic, *Int. J. Electrochem. Sci.*, **3**, 1 (2008).
2. M. Finsgar and I. Milosev, *Corros. Sci.*, **52**, 2737 (2010).
3. D.Y. Ryu and M.L. Free, *Anti-Corros. Methods Mater.*, **53**, 12 (2006).
4. R.T. Vashi, S.A. Desai and P.S. Desai, *Asian J. Chem.*, **20**, 4553 (2008).
5. G. Gece, *Corros. Sci.*, **50**, 2981 (2008).
6. A. Kokalj and S. Peljhan, *Langmuir*, **26**, 14582 (2010).
7. J.O. Mendes, E.C. da Silva and A.B. Rocha, *Corros. Sci.*, **57**, 254 (2012).
8. C.T. Lee, W.T. Yang and R.G. Parr, *Phys. Rev. B*, **37**, 785 (1988).
9. P.J. Hay and W.R. Wadt, *J. Chem. Phys.*, **82**, 270 (1985).
10. R.F.W. Bader, Atoms in Molecules: A Quantum Theory, Oxford University Press, New York (1994).
11. J.P. Perdew, K. Burke and M. Ernzerhof, *Phys. Rev. Lett.*, **78**, 1396 (1997).
12. P.J. Hay and W.R. Wadt, *J. Chem. Phys.*, **82**, 299 (1985).
13. B. Delley, *J. Chem. Phys.*, **113**, 7756 (2000).
14. J.R. Mohallem, T. de O. Coura, L.G. Diniz, G. de Castro, D. Assafrão and T. Heine, *J. Phys. Chem. A*, **112**, 8896 (2008).
15. R.L. Camacho-Mendoza, E. Aquino-Torres, J. Cruz-Borbolla, J.G. Alvarado-Rodríguez, O. Olvera-Neria, J. Narayanan and T. Pandiyan, *Struct. Chem.*, **25**, 115 (2014).
16. E.P. Yelsukov, E.V. Voronina and V.A. Barinov, *J. Magn. Magn. Mater.*, **115**, 271 (1992).
17. G. Autès, C. Barreteau, D. Spanjaard and M.-C. Desjonquères, *J. Phys. Condens. Matter*, **18**, 6785 (2006).
18. R. Soulairol, C.C. Fu and C. Barreteau, *J. Phys. Condens. Matter*, **22**, 295502 (2010).
19. E.S. Ferreira, C. Giacomelli, F.C. Giacomelli and A. Spinelli, *Mater. Chem. Phys.*, **83**, 129 (2004).
20. M. Tourabi, K. Nohair, M. Traisnel, C. Jama and F. Bentiss, *Corros. Sci.*, **75**, 123 (2013).
21. S.T. Zhang, Z.H. Tao, S.G. Liao and F.J. Wu, *Corros. Sci.*, **52**, 3126 (2010).
22. Y. Yan, W.H. Li, L.K. Cai and B.R. Hou, *Electrochim. Acta*, **53**, 5953 (2008).
23. E. Bayol, K. Kayakirilmaz and M. Erbil, *Mater. Chem. Phys.*, **104**, 74 (2007).
24. R. Saratha and R. Meenakshi, *Asian J. Chem.*, **25**, 1415 (2013).
25. M. Gholami, I. Danaee, M.H. Maddahy and M. RashvandAvei, *Ind. Eng. Chem. Res.*, **52**, 14875 (2013).
26. E.N. Dim, P.O. Ukoha and N.L. Obasi, *Asian J. Chem.*, **24**, 1899 (2012).
27. M. Ozcan, F. Karadag and I. Dehri, *Colloids Surf. A*, **316**, 55 (2008).
28. M. Hosseini, S.F.L. Mertens, M. Ghorbani and M.R. Arshadi, *Mater. Chem. Phys.*, **78**, 800 (2003).
29. E. McCafferty and N. Hackerman, *J. Electrochem. Soc.*, **119**, 146 (1972).
30. A. Lame (Galo), E. Kokalari (Teli) and A. Jano, *Asian J. Chem.*, **25**, 4017 (2013).
31. S. John and A. Joseph, *Mater. Corros.*, **64**, 625 (2013).
32. M. Finsgar, A. Lesar, A. Kokalj and I. Milosev, *Electrochim. Acta*, **53**, 8287 (2008).
33. T. Lu and F.W. Chen, *Acta Chim. Sin.*, **69**, 2393 (2011).
34. P. Macchi and A. Sironi, *Coord. Chem. Rev.*, **238-239**, 383 (2003).
35. E. Espinosa, I. Alkorta, J. Elguero and E. Molins, *J. Chem. Phys.*, **117**, 5529 (2002).
36. M. Eder, K. Terakura and J. Hafner, *Phys. Rev. B*, **64**, 115426 (2001).
37. S.K. Shukla and M.A. Quraishi, *Corros. Sci.*, **51**, 1007 (2009).
38. E.E. Oguzie, Y. Li, S.G. Wang and F. Wang, *RSC Adv.*, **1**, 866 (2011).
39. M. Ozcan, D. Toffoli, H. Ustunel and I. Dehri, *Corros. Sci.*, **80**, 482 (2014).
40. A. Doner, R. Solmaz, M. Ozcan and G. Kardas, *Corros. Sci.*, **53**, 2902 (2011).
41. S. John, B. Joseph, K.K. Aravindakshan and A. Joseph, *Mater. Chem. Phys.*, **122**, 374 (2010).